

## Enhanced Performance of Polymeric Bulk Heterojunction Solar Cells via Molecular Doping with TFSA

Yubin Xiao, Han Wang, Shuang Zhou, Keyou Yan, Zhiqiang Guan, Sai Wing Tsang, and Jianbin Xu

ACS Appl. Mater. Interfaces, Just Accepted Manuscript • Publication Date (Web): 03 Jun 2015

Downloaded from <http://pubs.acs.org> on June 4, 2015

### Just Accepted

"Just Accepted" manuscripts have been peer-reviewed and accepted for publication. They are posted online prior to technical editing, formatting for publication and author proofing. The American Chemical Society provides "Just Accepted" as a free service to the research community to expedite the dissemination of scientific material as soon as possible after acceptance. "Just Accepted" manuscripts appear in full in PDF format accompanied by an HTML abstract. "Just Accepted" manuscripts have been fully peer reviewed, but should not be considered the official version of record. They are accessible to all readers and citable by the Digital Object Identifier (DOI®). "Just Accepted" is an optional service offered to authors. Therefore, the "Just Accepted" Web site may not include all articles that will be published in the journal. After a manuscript is technically edited and formatted, it will be removed from the "Just Accepted" Web site and published as an ASAP article. Note that technical editing may introduce minor changes to the manuscript text and/or graphics which could affect content, and all legal disclaimers and ethical guidelines that apply to the journal pertain. ACS cannot be held responsible for errors or consequences arising from the use of information contained in these "Just Accepted" manuscripts.



ACS Publications

High quality. High impact.

ACS Applied Materials & Interfaces is published by the American Chemical Society.  
1155 Sixteenth Street N.W., Washington, DC 20036

Published by American Chemical Society. Copyright © American Chemical Society.  
However, no copyright claim is made to original U.S. Government works, or works  
produced by employees of any Commonwealth realm Crown government in the course  
of their duties.

# Enhanced Performance of Polymeric Bulk Heterojunction Solar Cells via Molecular Doping with TFSA

Yubin Xiao<sup>1</sup>, Han Wang<sup>1</sup>, Shuang Zhou<sup>1</sup>, Keyou Yan<sup>1</sup>, Zhiqiang Guan<sup>2</sup>, Sai-Wing Tsang<sup>2\*</sup>, Jianbin Xu<sup>1\*</sup>

<sup>1</sup>Department of Electronic Engineering and Materials Science and Technology Research Centre, The Chinese University of Hong Kong, Shatin, Hong Kong SAR, PR China.

<sup>2</sup> Department of Physics and Materials Science, The City University of Hong Kong, Kowloon Tong, Hong Kong SAR, PR China.

## Abstract

Organic solar cells based on bis(trifluoromethanesulfonyl)amide (TFSA,  $[CF_3SO_2]_2NH$ ) bulk doped poly[N-9“-hepta-decanyl-2,7-carbazole-alt-5,5-(4‘,7‘-di-2-thienyl-2‘,1‘,3‘-benzothiadiazole) (PCDTBT): C<sub>71</sub>-butyric acid methyl ester (PC<sub>71</sub>BM) were fabricated to study the effect of molecular doping. By adding TFSA (0.2 ~ 0.8 wt%, TFSA to PCDTBT) in the conventional PCDTBT:PC<sub>71</sub>BM blends, we found that the hole mobility was increased with the reduced series resistance in photovoltaic devices. The p-doping effect of TFSA was confirmed by photoemission spectroscopy that the Fermi level of doped PCDTBT shifts downward to the HOMO level and it results in a larger internal electrical field at the donor/acceptor interface for more efficient charge transfer. Moreover, the doping effect was also confirmed by charge modulated electroabsorption spectroscopy (CMEAS), showing that there are additional polaron signals in the sub-bandgap region in the doped thin films. With decreased series resistance, the open-circuit voltage ( $V_{oc}$ ) was increased from 0.85 V to 0.91 V and the fill factor (FF) was

\* Corresponding author: [jbxu@ee.cuhk.edu.hk](mailto:jbxu@ee.cuhk.edu.hk) (J.B. Xu)

\* Co-corresponding author: [saitang@cityu.edu.hk](mailto:saitang@cityu.edu.hk) (S.-W. Tsang)

improved from 60.7 % to 67.3 %, resulting in a largely enhanced power conversion efficiency (PCE) from 5.39 % to 6.46 %. Our finding suggests the molecular doping by TFSA can be a facile approach to improve the electrical properties of organic materials for future development of organic photovoltaic devices (OPVs).

Keywords:

Polymer solar cells; TFSA doping ; charge transfer; carrier mobility; Fermi level.

## 1. Introduction

Organic photovoltaic has been an emerging technology during the last two decades due to its potential for low-cost fabrication and high efficiency.<sup>1</sup> Particularly, solution processable polymeric bulk heterojunction (BHJ) architecture has gained lots of attentions due to the ease of fabrication processes. In the BHJ structure, an electron donating polymer and an electron acceptor (usually fullerene derivatives) are mixed together to form a nanoscale binary phase separation and bi-continuous interpenetration network, which has significant contribution on facilitating efficient exciton dissociation.<sup>2</sup> Recently, the power conversion efficiency (PCE) of single BHJ solar cells has reported over 10 % in solution processable solar cells which is approaching the threshold of 15 % for commercialization.<sup>3</sup> Therefore, great effort is devoted to further improving the performance of polymer solar cells. The major drawbacks of BHJ-OPVs are often attributable to narrow light absorption band of the polymers, limited exciton migration, and low charge-carrier mobility. Hence, a relatively low open circuit voltage ( $V_{oc}$ ) and a low fill factor (FF) are often observed in such organic solar cells. As  $V_{oc}$  is depended on the energy gap between the lowest unoccupied molecular orbital (LUMO) of the acceptor and the highest occupied molecular orbital (HOMO) of the donor polymer, one strategy to increase the  $V_{oc}$  is to develop new polymers with relatively low-lying HOMO level, such as PCDTBT,<sup>4-8</sup> benzodithiophene polymers (PTBs)<sup>9, 10</sup>etc. Another approach is to optimize the energetic alignment at the electrode/active layer interface to create an Ohmic contact, to reduce the charge recombination and to promote carrier collection<sup>11</sup>. Moreover, ternary solar cells have been developed to further enhance PCE by expanding the light absorption range and smooth the energy level at the BHJ interface.<sup>12-14</sup>

It has been demonstrated that the electrical properties of the semi-conducting polymers can be modified via molecular doping with charge transfer between the organic host and dopant molecules.<sup>15-17</sup> And molecular doping has also been applied to enhance the photoconductivity and charge injection/collection efficiencies in BHJ-OPVs.<sup>18-21</sup> However, the choices of the dopant molecules used in polymeric materials are limited, as it requires good compatibility in solubility and efficient charge transfer. When doped with a prototypical p-type molecular dopant tetrafluoro-tetracyanoquinodimethane (F4-TCNQ), a doped polymer showed downward shifted Fermi level and increased carried density, as a result, the background hole carrier concentration was increased, contributing to an increased photoconductivity and a resultant improved PCE.<sup>19,22</sup> Another p-type dopant, molybdenum tris[1-(methoxycarbonyl)-2-(trifluoromethyl)-ethane-1,2-dithiolene] ( $\text{Mo}(\text{tfd}-\text{CO}_2\text{Me})_3$ ), has also been proven to be able to create an efficient hole-collecting contact in solution-processed inverted polymer solar cells<sup>11</sup>. Recently, a new dopant bis(trifluoromethanesulfonyl)amide (TFSA) has also been reported as a p-type dopant for carbonaceous materials (carbon nanotube, graphene) due to its strong electron affinity. A graphene-based Schottky junction solar cells doped with TFSA exhibited a PCE of 8.6 %.<sup>23</sup> In addition, in polymer light emitting diodes, the work function of graphene electrode was successfully increased by TFSA for efficient hole injection.<sup>24</sup>

In this contribution, we investigated the application of TFSA as molecular dopant in solution-processed BHJ-OPVs. By controlling the doping concentration (0.2~0.8 wt%, TFSA to PCDTBT), we found that the  $V_{oc}$  of the PCDTBT:PC<sub>71</sub>BM solar cells was increased from 0.85 V to 0.91 V, FF was increased from 60.7% to 67.3% and an enhanced PCE from 5.39% to 6.46% was further achieved. Employing different spectroscopy techniques, we found that there is efficient charge transfer between PCDTBT and TFSA, which enables the modification of electrical properties and energy level alignment in the photovoltaic devices. The results demonstrate the capability of TFSA as an efficient molecular dopant used in polymeric BHJ-OPVs.

## 2. Experimental section

PCDTBT, PC<sub>71</sub>BM and TFSA were purchased from 1-Material Chemscitech, Inc., Lumitec and Sigma-Aldrich respectively, and used as received. In order to demonstrate the effect of TFSA, the device with configuration of ITO (180 nm)/PEDOT:PSS(40 nm)/PCDTBT:PC<sub>71</sub>BM

(~80 nm)/LiF (1 nm)/Al (100 nm) were fabricated. To begin, a pre-patterned ITO (conductivity: 10~15  $\Omega/\text{square}$ ) glass was cleaned by detergent, deionized water, acetone and isopropanol in sequence, followed by oxygen plasma treatment for 90 s. A thin hole injection layer of PEDOT:PSS was spun-cast onto pre-cleaned ITO glass with a thickness of ca. 40 nm, and then annealed at 145 °C for 10 min in air. PCDTBT and PC<sub>71</sub>BM with a mass ratio of 1:3 were dissolved in a mixed solution composed of 1,2 o-dichlorobenzene (o-DCB) and chloroform (CF) (1:1 vol) with a total concentration of 29 mg/ml. TFSA was dissolved in 1 ml 1,2 o-dichlorobenzene (o-DCB) and chloroform (CF) (1:1) mixed solvent and then it was added to PCDTBT :PC<sub>71</sub>BM blends with desired amount. The weight ratio of TFSA to PCDTBT is 0.2%, 0.4%, 0.6% and 0.8%. The mixed solution was then spun-cast atop the pre-coated PEDOT:PSS layer to form the active layer, giving rise to a thickness of ~80 nm. Following that, 20 min soft annealing and a further annealing at 120 °C for 10 min were conducted. Finally, a thin LiF interfacial layer (~1 nm) and a 100 nm thick Al electrode were deposited sequentially by thermal evaporation. The evaporator was BOC Edwards Auto 306 and the active layer area of the device was defined by a shadow mask of 2 mm × 6 mm.

Electrical measurements were performed by a semiconductor characterization system (Keithley 236) at room temperature in air under the spectral output from solar simulator (Newport) using an AM 1.5G filter with a light power of 100 mW/cm<sup>2</sup>. The light intensity was precisely calibrated by a calibrated silicon solar cell. The morphologies of the PCDTBT:PC<sub>71</sub>BM blend thin films were characterized by atomic force microscopy (AFM) in tapping mode (Dimension icon scanasyst). The thickness of the active layer and evaporated layers were recorded with a thickness monitor (Sigma SQM-160), and also verified by AFM. The impedance were measured in a frequency range from 0.1 Hz to 1 M Hz (CHI 760). The admittance, capacitance-voltage ( $C-V$ ) and capacitance-frequency ( $C-F$ ) characteristics were measured by HP Hewlett packard 4248A. Especially in  $C-F$  measurement, a very thick PCDTBT layer (500 nm) were prepared in order to sweep out the relaxation peak in the  $-\Delta B$  vs  $f$  plots. UPS measurement was also conducted, and the Fermi energy level of PCDTBT is determined by  $E = h\nu - E_{\text{onset}}$ , where  $h\nu$  is the energy of the ultraviolet irradiation with the value of 21.22 eV. A -5 V bias voltage was applied on ITO electrode in order to separate the low cut-off energy levels of the secondary photo-electrons from the spectra edge of UPS. The testing devices for CMEAS have the structure of ITO/PCDTBT/LiF/Al and the measurements were carried out at room temperature. A

monochromatic parallel beam probed the devices through the ITO side with an incident angle of 45° and was reflected by the back Al electrode. Calibrated silicon and germanium photodetectors were used to detect the reflected signals.

### 3. Results and Discussion

Figure 1a shows the materials in the study and the doping process is illustrated in Figure 1b, after the addition of TFSA to PCDTBT:PC<sub>71</sub>BM blends, the electron will transfer from PCDTBT to TFSA due to the strong electron affinity of TFSA. Because of the electron lost in PCDTBT, the work function of PCDTBT will move downward and closer to its HOMO energy level as indicated by the green arrow. As a result, the hole concentration in the donor polymer will increase. Such phenomenon is confirmed by *C-V* characteristics and photoemission spectroscopy measurement that will be discussed later.

The influence of TFSA dopants on the morphological properties of the photoactive layer was examined by atomic force microscopy (AFM). Figure 2 shows the 2 μm × 2 μm AFM topographic images of bare PCDTBT:PC<sub>71</sub>BM films as well as the TFSA-doped films (0.2% to 0.8%). For pristine PCDTBT:PC<sub>71</sub>BM, it shows very smooth and featureless structure with a low root mean square (RMS) value of 0.49 nm. While for doped films, the RMS displays slightly increased value to 0.50, 0.51, 0.52 and 0.53 nm at each doping concentration, respectively. And the minor variation of the film morphology would have neglectable impact to the polymer film properties. From the corresponding phase images (Figure S1), no obvious ternary TFSA domain was observed, indicating small dopant concentration would not change the PCDTBT:PC<sub>71</sub>BM interpenetrating network. Although AFM is only a surface sensitive technique, it provides useful insight of the bulk information of the active layers. From the above morphological and phase images, we can expect that the variation of the photoactive layer properties could be neglected at low doping concentration due to the near unchanged film construction.

Next, we studied the influence of molecular doping by TFSA on the performance of photovoltaic effect. Figure 3a shows typical current density versus voltage (*J-V*) characteristics of PCDTBT:PC<sub>71</sub>BM solar cells under AM 1.5 G illumination. For pristine PCDTBT:PC<sub>71</sub>BM solar cells, it displays a  $V_{oc}$  of 0.85 V, a short circuit current ( $J_{sc}$ ) of 10.5 mA/cm<sup>2</sup> and a FF of 60.7% and all of the above give rise to a PCE of 5.39%. With addition of TFSA, a noticeable enhancement of  $V_{oc}$  and FF are observed, while  $J_{sc}$  is insensitive to the TFSA doping at various

concentrations. The detailed device characteristics are listed in Table 1. In the device adding only 0.2% TFSA, the  $V_{oc}$  is increased to 0.89 V and FF is increased to 63.0%. When adding 0.4% TFSA, the device reaches its optimized performance with a  $V_{oc}$  of 0.91 V, a FF of 67.3% and a PCE to 6.46%. As discussed previously, the doped PCDTBT has a low work function due to electron transfer to TFSA and results in an optimized energy level alignment, thus the charge injection barrier could therefore be reduced at the ITO-active layer interface. To further confirm the enhancement at lower doping concentration, devices with and without the optimized condition of 0.4% TFSA dopant (both devices without PEDOT:PSS hole injection layer) were fabricated (see Figure S2 in supporting information). Similarly, the  $V_{oc}$  was increased from 0.40 to 0.58 V and FF increased slightly from 42.9% to 44.0%. The results of this simple device structure without hole transporting layer (HTL) confirmed that the doped device provided a better charge transfer path across the electrode-active layer junction due to the reduced charge injection barrier. However, when increasing the dopant concentration to 0.6% and 0.8%, the devices performance rolled-off, this is similar to the previous report that the low to medium doping concentration reduced the carrier mobility<sup>25, 26</sup>.

Figure 3b shows the dark current versus bias voltage characteristics of the PV devices. At low doping concentrations, the dark current at reverse bias and leakage current at zero bias are obviously reduced, which significantly increases the diode rectifying ratios by 2 orders of magnitude. The decreased dark current indicates a larger shunt resistance ( $R_{sh}$ ) that could prevent the current from leakage and hence increase the  $V_{oc}$  and FF. While for the dark current in the forward bias region (1-2 V) that dominated by fast carriers of electrons, the currents are barely changed, indicating that doping in PCDTBT:PC<sub>71</sub>BM films with low dopant concentrations does not affect the electron transportation. Previous works have also shown that a low doping molecular concentration had less impact on the carrier transportation and the enhanced carrier concentration would not lead to a detrimental charge recombination<sup>22, 27</sup>.

Molecular doping with extra carriers would lead to lower resistance in PV devices. Figure 4 shows the Nyquist curves of the impedance spectra for undoped and doped PCDTBT:PC<sub>71</sub>BM PV devices measured at the open circuit voltage condition. An apparent change is observed in the doped devices. The real impedance is decreased from 1011 Ω to 918Ω, 352Ω and 701 Ω at doping concentrations are increased from 0.2 wt% to 0.6 wt%, respectively. This can be attributed to the contribution of both carrier concentration and carrier mobility. In order to

further investigate the impact of molecular doping on the electrical properties of PCDTBT:PC<sub>71</sub>BM solar cells, we used admittance spectroscopy to measure the carrier mobility and carrier transit time in those devices<sup>28, 29</sup>. The carrier mobility can be exacted from the relation of  $\mu_{dc} = d^2/(\tau_{dc}V_{dc})$ , where  $d$  is the thickness of the polymer and  $V_{dc}$  is the external applied bias voltage. Hence, from the relationship mentioned above, the carrier mobility and transit time can be extracted. The hole-only devices were fabricated with structure of ITO/PEDOT:PSS/PCDTBT/MoO<sub>3</sub>/Al. MoO<sub>3</sub> is an electron blocking layer in here. Figure 5 (a,b,c) and (d,e,f) present the impedance analysis of control and 0.4 % TFSA doped devices with a bias voltage range from 3 to 12 V respectively. Apparently, the doped devices display an enhanced conductance at each voltage bias. The results are summarized in Table 2. Taking the typical bias  $V_{dc}$  at 10 V as an example, the carrier mobility is increased from  $6.7 \times 10^{-4}$  to  $8.9 \times 10^{-4}$  cm<sup>2</sup>/Vs, and the conductance from 37 to 150  $\mu$ S. The higher carrier mobility in the slightly doped device suggests more efficient charge extraction.

To confirm the increased carrier mobility, *J-V* characteristics was conducted in a bias voltage range of 0-10 V (Figure S3) for undoped and doped PCDTBT:PC<sub>71</sub>BM hole only devices. With positive bias applied on ITO anode, holes are injected into PCDTBT and the space charge limited current (SCLC) occurs.<sup>30</sup> And the mobility can be extracted from Mott-Gurney equation:

$$\mu = \frac{8d^3}{9\varepsilon_0\varepsilon_r} \left( \frac{\sqrt{J}}{V_a} \right)^2, \text{ where } \mu \text{ is the carrier mobility, } d \text{ is the active layer thickness, } \varepsilon_0 \text{ (} 8.85 \times 10^{-12} \text{ F/m) and } \varepsilon_r \text{ (equal to 3 for organic materials) are the permittivity of vacuum and relative permittivity respectively. According to the above equation, the hole mobility of control device is } 6.2 \times 10^{-4} \text{ cm}^2/\text{Vs and after adding TFSA, the hole mobility is gradually increased. With 0.4 % TFSA doped, the hole mobility achieves } 9.2 \times 10^{-4} \text{ cm}^2/\text{Vs which is in good agreement with the admittance analysis results. However, when the doping concentration is increased to 0.8 %, the hole mobility is decreased to } 5.9 \times 10^{-4} \text{ cm}^2/\text{Vs compared to the undoped device. This decreasing tendency is rationalized by an analytic model of carrier mobility in doped organic semiconductors by D.Heher et al.}<sup>25</sup> To explore the doping effect of TFSA on PCDTBT, the UPS measurements were carried out at various concentrations and the results are shown in Figure 6. The cut-off energy level of TFSA doped PCDTBT shifts from 15.90 eV to lower binding energy level of 15.85 eV at 0.2 % and saturates at 15.73 eV for the rest of the doping concentrations (0.4 % to 0.8 %), suggesting an increase of work function from 5.32 to 5.37 eV and 5.49 eV,$$

1  
2  
3 respectively. Because the HOMO level of PCDTBT is around 5.5 eV, it clearly shows that after  
4 doping with TFSA, the Fermi level of PCDTBT shifts downward effectively and leads to a larger  
5 effective bandgap at the donor/acceptor interface, and the enlarged effective bandgap should be  
6 one of the reasons for the increased open circuit voltage.  
7  
8

9  
10 In order to extract the carrier concentration, we measured the capacitance-voltage  
11 characteristic of the devices and compared the result with the Mott-Schottky relation:  $C^2 = 2$   
12  $(V_{bi} - V)/A^2 q \epsilon_0 \epsilon_r N_A$ , where A is the device area ( $0.12 \text{ mm}^2$ ),  $\epsilon_r$  and  $\epsilon_0$  are the relative dielectric  
13 constant and permittivity of vacuum respectively,  $q$  the elementary charge,  $N_A$  the concentration  
14 of impurities. Figure 7 shows the C-V characteristics and Mott-Schottky curves of  
15 PCDTBT:PC<sub>71</sub>BM solar cells with and without TFSA doping at various concentrations. Having  
16 similar device thickness, higher capacitance is obtained after doping with TFSA as shown in  
17 Figure 7 (a). It suggests a higher carrier concentration corresponding to charge transfer between  
18 TFSA and PCDTBT. It should also be noted that, the increased built-in potential ( $V_{bi}$ ) after  
19 doping with TFSA is in good agreement with the improved  $V_{oc}$  in PV devices as shown above.  
20 We extract the carrier concentration from the linear region from the plots with different doping  
21 ratios. For pristine PCDTBT:PC<sub>71</sub>BM device, we obtain  $N_A$  at around  $1.0 \times 10^{17} \text{ cm}^{-3}$ , and in 0.2  
22 % TFSA doped device,  $N_A$  is increased to  $1.7 \times 10^{17} \text{ cm}^{-3}$  and thereafter  $N_A$  is keeping increased  
23 as more TFSA added. The carrier concentrations for each doping concentration are summarized  
24 in Table 1, which  $N_A$  is proportional to the doping concentration.  
25  
26

27 To further figure out the doping effect of TFSA in PCDTBT, charge modulated  
28 electroabsorption spectroscopy (CMEAS) was employed to investigate the change of absorption  
29 due to additional polaron states in the doped devices.<sup>31, 32</sup> In CMEAS measurement, by  
30 measuring the electroabsorption (EA) signal that induced by charge-modulation (CM) in the  
31 polymer, a clear sub-bandgap signal through direct excitation of excitons to the charge transfer  
32 states can be observed. Therefore, if there is charge transfer between TFSA and PCDTBT, the  
33 photo-generated carriers will couple with the modulating electric field and generate subtle  
34 changes in the optical absorption cross section in the sub-bandgap region, where an additional  
35 sub-bandgap signal in the infrared region should be observed in CMEAS measurement. Figure  
36 8(a) shows the CMEAS spectra of pristine PCDTBT and TFSA doped PCDTBT films. The  
37 excitonic feature of PCDTBT appearing above 1.8 eV is ascribed to the Stark effect due to the  
38 coupling between the excitonic level (1B<sub>u</sub>) and the higher forbidden states under the applied  
39 electric field.  
40  
41

1  
2  
3 electric field. In the doped PCDTBT device (Figure 8(b)), additional polaron signals in the sub-  
4 bandgap region from 1.0 eV to 1.8 eV are observed. This further confirms the efficient charge  
5 transfer between TFSA and PCDTBT.  
6  
7

8 Finally, we demonstrated the capability of molecular doping using TFSA in different polymer  
9 solar cells. Figure S4 shows the *J-V* characteristics of solar cells based on poly(3-  
10 hexylthiophene-2,5-diyl) (P3HT) : (PC<sub>61</sub>BM). Having a doping concentration of 0.4 %, an  
11 increased  $J_{sc}$  from 9.01 mA/cm<sup>2</sup> to 9.36 mA/cm<sup>2</sup> and an  $V_{oc}$  from 0.60 V to 0.63 V are observed.  
12 As a result, the final PCEs are increased from 3.42 % to 3.76 % by doping with TFSA. The  
13 doping effect to polymer light absorption for both donors were investigated as well (Figure S5),  
14 it can be seen that after mixing with TFSA, the light absorption shows very similar tendency,  
15 indicating that the polymer structure are not affected by the dopant.  
16  
17  
18  
19  
20  
21  
22  
23  
24

#### 25 **4. Conclusion**

26 In summary, our TFSA-doped PCDTBT:PC<sub>71</sub>BM solar cell has significant improvement  
27 in both open circuit voltage and fill factor, leading to an improvement of PCEs from 5.39% to  
28 6.46%. Impedance spectroscopy and admittance spectroscopy prove that the doped devices have  
29 higher carrier concentration and concentration dependent carrier mobility. Photoemission  
30 spectroscopy results show the downward shifting of the Fermi level of PCDTBT after doping.  
31 Such charge transfer has also been confirmed by charge modulation spectroscopy that addition  
32 polaron states are induced after doping. Our results demonstrate that TFSA can be used as an  
33 efficient doping molecule to further optimize the electrical properties of the polymeric based  
34 bulk heterojunction photovoltaic devices.  
35  
36  
37  
38  
39  
40  
41  
42  
43  
44

#### 45 **Acknowledgements**

46 This work is in part supported by Research Grants Council of Hong Kong, particularly, via  
47 Grant Nos CUHK2/CRF/08, CUHK4182/09E, CUHK4179/10E, N-CUHK405/12 and  
48 AoE/P-03/08. J.B Xu would like to thank the National Science Foundation of China for the  
49 support, particularly, via Grant No. 61229401. S-W Tsang would like to thank RGC-  
50 20101514 and CityU-9610309. We thank Dr. Fangyan Xie of instrumental analysis and  
51 research center, Sun Yat-sen University for the UPS measurement.  
52  
53  
54  
55  
56  
57  
58  
59  
60

## Supporting Information

AFM phase images of PCDTBT:PC<sub>71</sub>BM film; *J-V* characteristics of PCDTBT:PC<sub>71</sub>BM without PEDOT:PSS; SCLC mobility; *J-V* characteristics of P3HT:PC<sub>61</sub>BM solar cells; UV-vis spectroscopy and EQE. This supporting information is available free of charge via the Internet at <http://pubs.acs.org>.

## References

1. Roncali, J.; Leriche, P.; Blanchard, P. Molecular Materials for Organic Photovoltaics: Small is Beautiful. *Adv. Mater.* 2014, 26, 3821-3838.
2. Son, H. J.; Carsten, B.; Jung, I. H.; Yu, L. Overcoming Efficiency Challenges in Organic Solar Cells: Rational Development of Conjugated Polymers. *Energy Environ. Sci.* 2012, 5, 8158-8170.
3. Liu, Y.H.; Li, Z.J.; Mu, C.; Ma, W.; Hu, H.; Jiang, K.; Lin, H.R.; Ade, H.; Yan, H. Aggregation and Morphology Control Enables Multiple Cases of High-Efficiency Polymer Solar Cells. *Nat. Commun.* 2014, 5, 5293-5300.
4. Jia, X.; Shen, L.; Yao, M. N.; Liu, Y.; Yu, W. J.; Guo, W. B.; Ruan, S. P. Highly Efficient Low-Bandgap Polymer Solar Cells with Solution-Processed and Annealing-Free Phosphomolybdic Acid as Hole-Transport Layers. *AcS Appl. Mater. Inter.* 2015, 7, 5367-5372.
5. Yu, W. J.; Shen, L.; Shen, P.; Long, Y. B.; Sun, H. W.; Chen, W. Y.; Ruan, S. P. Semitransparent Polymer Solar Cells with 5% Power Conversion Efficiency Using Photonic Crystal Reflector. *ACs Appl. Mater. Inter.* 2014, 6, 599-605.
6. Tong, M. H.; Coates, N. E.; Moses, D.; Heeger, A. J.; Beaupre, S.; Leclerc, M. Charge Carrier Photogeneration and Decay Dynamics in the Poly(2,7-carbazole) Copolymer PCDTBT and in Bulk Heterojunction Composites with PC<sub>70</sub>BM. *Phys. Rev. B* 2010, 81, 12510.
7. Wakim, S.; Beaupre, S.; Blouin, N.; Aich, B. R.; Rodman, S.; Gaudiana, R.; Tao, Y.; Leclerc, M. Highly Efficient Organic Solar Cells Based on a Poly(2,7-carbazole) Derivative. *J. Mater. Chem.* 2009, 19, 5351-5358.
8. Wenjuan Yu, X. J., Yongbing Long, Liang Shen, Yan Liu, Wenbin Guo, Shengping Ruan. Highly Efficient Semitransparent Polymer Solar Cells with Color Rendering Index Approaching 100 Using One-Dimensional Photonic Crystal. *ACs Appl. Mater. Inter.* 2015, 10.1021/acsami.5b02039.
9. Lu, L. Y.; Yu, L. P. Understanding Low Bandgap Polymer PTB7 and Optimizing Polymer Solar Cells Based on It. *Adv. Mater.* 2014, 26, 4413-4430.
10. Liang, Y. Y.; Xu, Z.; Xia, J. B.; Tsai, S. T.; Wu, Y.; Li, G.; Ray, C.; Yu, L. P. For the Bright Future-Bulk Heterojunction Polymer Solar Cells with Power Conversion Efficiency of 7.4%. *Adv. Mater.* 2010, 22, E135-E138.
11. Dai, A.; Zhou, Y. H.; Shu, A. L.; Mohapatra, S. K.; Wang, H.; Fuentes-Hernandez, C.; Zhang, Y. D.; Barlow, S.; Loo, Y. L.; Marder, S. R.; Kippelen, B.; Kahn, A. Enhanced Charge-Carrier Injection and Collection Via Lamination of Doped Polymer Layers p-Doped with a Solution-Processible Molybdenum Complex. *Adv. Funct. Mater.* 2014, 24, 2197-2204.

- 1  
2  
3  
4  
5  
6  
7  
8  
9  
10  
11  
12  
13  
14  
15  
16  
17  
18  
19  
20  
21  
22  
23  
24  
25  
26  
27  
28  
29  
30  
31  
32  
33  
34  
35  
36  
37  
38  
39  
40  
41  
42  
43  
44  
45  
46  
47  
48  
49  
50  
51  
52  
53  
54  
55  
56  
57  
58  
59  
60
12. An, Q. S.; Zhang, F. J.; Li, L. L.; Wang, J.; Sun, Q. Q.; Zhang, J.; Tang, W. H.; Deng, Z. B. Simultaneous Improvement in Short Circuit Current, Open Circuit Voltage, and Fill Factor of Polymer Solar Cells through Ternary Strategy. *ACS Appl. Mater. Inter.* 2015, 7, 3691-3698.
  13. Khlyabich, P. P.; Burkhart, B.; Thompson, B. C. Compositional Dependence of the Open-Circuit Voltage in Ternary Blend Bulk Heterojunction Solar Cells Based on Two Donor Polymers. *J. Am. Chem. Soc.* 2012, 134, 9074-9077.
  14. Ameri, T.; Min, J.; Li, N.; Machui, F.; Baran, D.; Forster, M.; Schottler, K. J.; Dolfen, D.; Scherf, U.; Brabec, C. J. Performance Enhancement of the P3HT/PCBM Solar Cells through NIR Sensitization Using a Small-Bandgap Polymer. *Adv. Energy Mater.* 2012, 2, 1198-1202.
  15. Li, X.M.; Xie, D.; Park, H.S.; Zhu, M. T. H. Z.; Wang, K.L.; Wei, J.Q.; Wu, D.H.; Zhu, J. K. Ion Doping of Graphene for High-Efficiency Heterojunction Solar Cells. *Nanoscale* 2013, 5, 1945-1948.
  16. Kim, S. M.; Jo, Y. W.; Kim, K. K.; Duong, D. L.; Shin, H. J.; Han, J. H.; Choi, J. Y.; Kong, J.; Lee, Y. H. Transparent Organic P-Dopant in Carbon Nanotubes: Bis(trifluoromethanesulfonyl)imide. *ACS Nano* 2010, 4, 6998-7004.
  17. Zhou, Y. H.; Fuentes-Hernandez, C.; Shim, J.; Meyer, J.; Giordano, A. J.; Li, H.; Winget, P.; Papadopoulos, T.; Cheun, H.; Kim, J.; Fenoll, M.; Dindar, A.; Haske, W.; Najafabadi, E.; Khan, T. M.; Sojoudi, H.; Barlow, S.; Graham, S.; Bredas, J. L.; Marder, S. R.; Kahn, A.; Kippelen, B. A Universal Method to Produce Low-Work Function Electrodes for Organic Electronics. *Science* 2012, 336, 327-332.
  18. Zhou, H.Q.; Y. Z., Mai, C.K.; Collins, S.D.; Nguyen, T.Q.; Bazan, G.C.; Heeger, A.J. Conductive Conjugated Polyelectrolyte as Hole-Transporting Layer for Organic Bulk Heterojunction Solar Cells. *Adv. Mater.* 2014, 26, 780-785.
  19. Han, X.; Wu, Z.; Sun, B. Enhanced Performance of Inverted Organic Solar Cell by a Solution-Based Fluorinated Acceptor Doped P3HT:PCBM Layer. *Org. Electron.* 2013, 14, 1116-1121.
  20. Tunc, A. V.; De Sio, A.; Riedel, D.; Deschler, F.; Da Como, E.; Parisi, J.; von Hauff, E. Molecular Doping of Low-Bandgap-Polymer:Fullerene Solar Cells: Effects on Transport and Solar Cells. *Org. Electron.* 2012, 13, 290-296.
  21. Lei, X.; Zhang, F.; Song, T.; Sun, B. P-type Doping Effect on the Performance of Organic-Inorganic Hybrid Solar Cells. *Appl. Phys. Lett.* 2011, 99, 233305-3.
  22. Zhang, Y.; Zhou, H.Q.; Seifter, J.; Ying, L.; Mikhailovsky, A.; Heeger, A.J.; Bazan, G.C.; Nguyen, T.Q. Molecular Doping Enhances Photoconductivity in Polymer Bulk Heterojunction Solar Cells. *Adv. Mater.* 2013, 25(48), 7038-7044.
  23. Miao, X. C.; Tongay, S.; Petterson, M. K.; Berke, K.; Rinzler, A. G.; Appleton, B. R.; Hebard, A. F. High Efficiency Graphene Solar Cells by Chemical Doping. *Nano Lett.* 2012, 12, 2745-2750.
  24. Kim, D.; Lee, D.; Lee, Y.; Jeon, D. Y. Work-Function Engineering of Graphene Anode by Bis(trifluoromethanesulfonyl)amide Doping for Efficient Polymer Light-Emitting Diodes. *Adv. Funct. Mater.* 2013, 23, 5049-5055.
  25. Arkhipov, V. I.; Emelianova, E. V.; Heremans, P.; Bassler, H. Analytic Model of Carrier Mobility in Doped Disordered Organic Semiconductors. *Phys. Rev. B* 2005, 72, 235202.
  26. Pingel, P.; Schwarzl, R.; Neher, D. Effect of Molecular P-doping on Hole Density and Mobility in poly(3-hexylthiophene). *Appl. Phys. Lett.* 2012, 100, 143303.
  27. Xiao, Y.B.; Zhou, S.; Su, Y.R.; Ye, L.; Tsang, S.W.; Xie, F.Y.; Xu, J.B. TFSA Doped Interlayer for Efficient Organic Solar Cells. *Org. Electron.* 2014, 15, 3702-3709.
  28. Tsang, S. W.; Tse, S. C.; Tong, K. L.; So, S. K. PEDOT : PSS Polymeric Conducting Anode for Admittance Spectroscopy. *Org. Electron.* 2006, 7, 474-479.
  29. Tsang, S. W.; So, S. K.; Xu, J. B. Application of Admittance Spectroscopy to Evaluate Carrier Mobility in Organic Charge Transport Materials. *J. Appl. Phys.* 2006, 99, 013706.

- 1  
2  
3 30. Lee, H. K. H.; Li, Z.; Constantinou, I.; So, F.; Tsang, S. W.; So, S. K. Batch-to-Batch Variation of  
4 Polymeric Photovoltaic Materials: its Origin and Impacts on Charge Carrier Transport and Device  
5 Performances. *Adv. Energy. Mater.* 2014, 4, 1400768-8  
6  
7 31. Chen, S.; Tsang, S. W.; Lai, T. H.; Reynolds, J. R.; So, F. Dielectric Effect on the Photovoltage Loss  
8 in Organic Photovoltaic Cells. *Adv. Mater.* 2014, 26, 6125-6131.  
9  
10 32. Tsang, S. W.; Chen, S.; So, F. Energy Level Alignment and Sub-Bandgap Charge Generation in  
11 Polymer:Fullerene Bulk Heterojunction Solar Cells. *Adv. Mater.* 2013, 25, 2434-2439.  
12  
13  
14  
15  
16  
17  
18  
19  
20  
21  
22  
23  
24  
25  
26  
27  
28  
29  
30  
31  
32  
33  
34  
35  
36  
37  
38  
39  
40  
41  
42  
43  
44  
45  
46  
47  
48  
49  
50  
51  
52  
53  
54  
55  
56  
57  
58  
59  
60

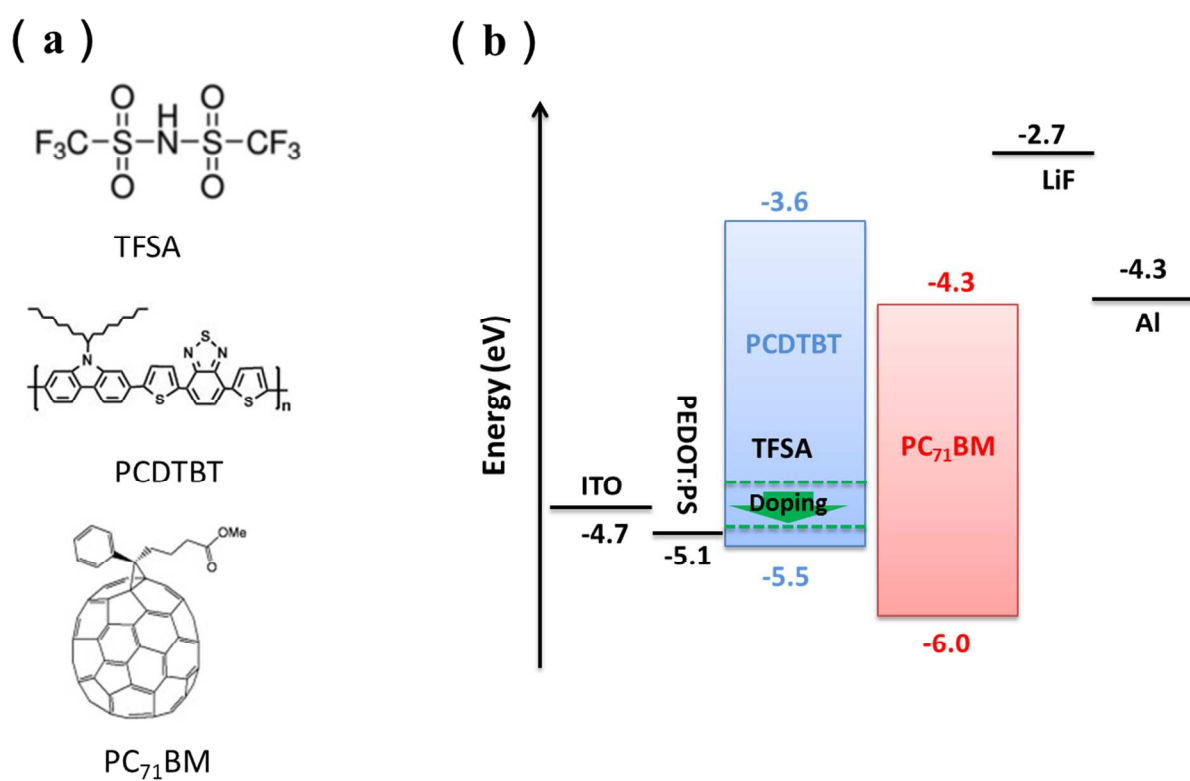


Figure 1. (a) Chemical structure of TFSA, PCDTBT, PC<sub>71</sub>BM used in the study. (b) Energy diagram of the BHJ solar cell. With the p-type doping, the green arrow indicates the Fermi level of PCDTBT shifted towards its HOMO level.

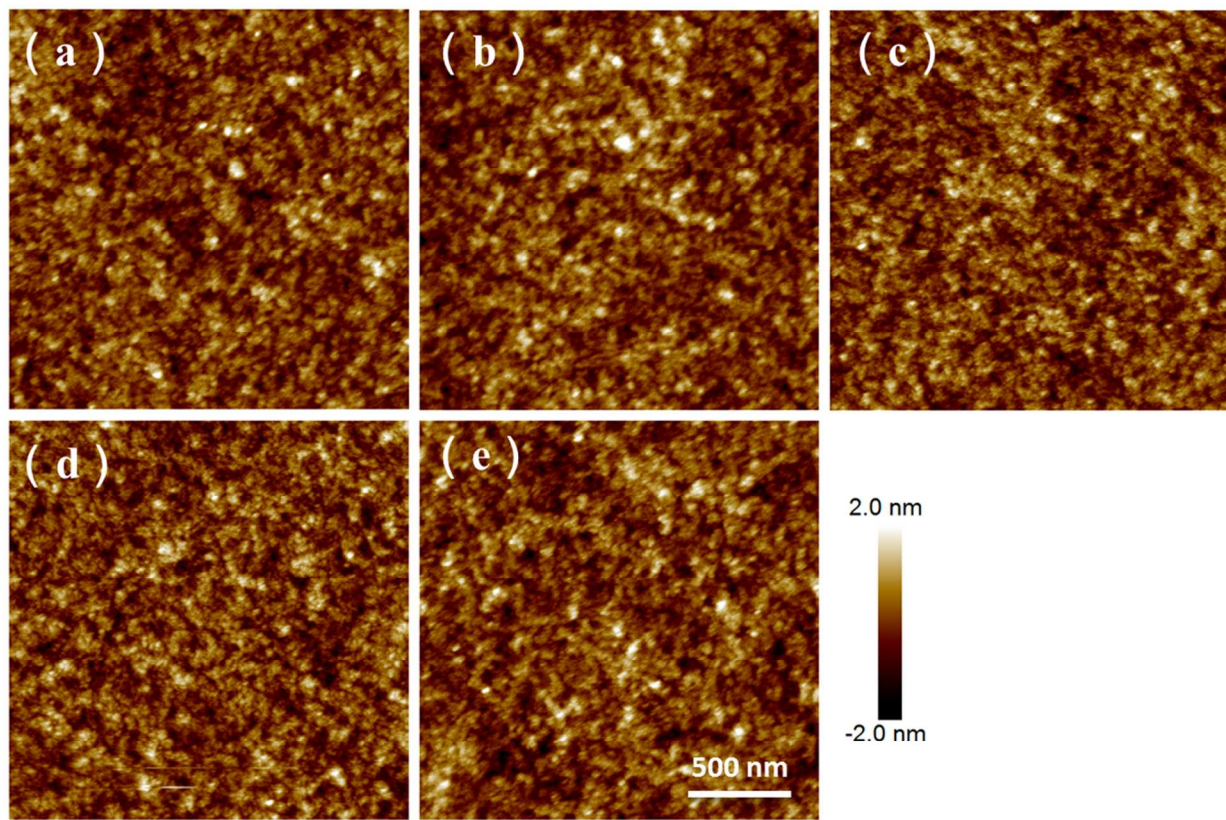


Figure 2. AFM morphology images of PCDTBT:PC<sub>71</sub>BM, (a) pristine and with (b) 0.2%, (c) 0.4%, (d) 0.6%, (e) 0.8% TFSA dopant.

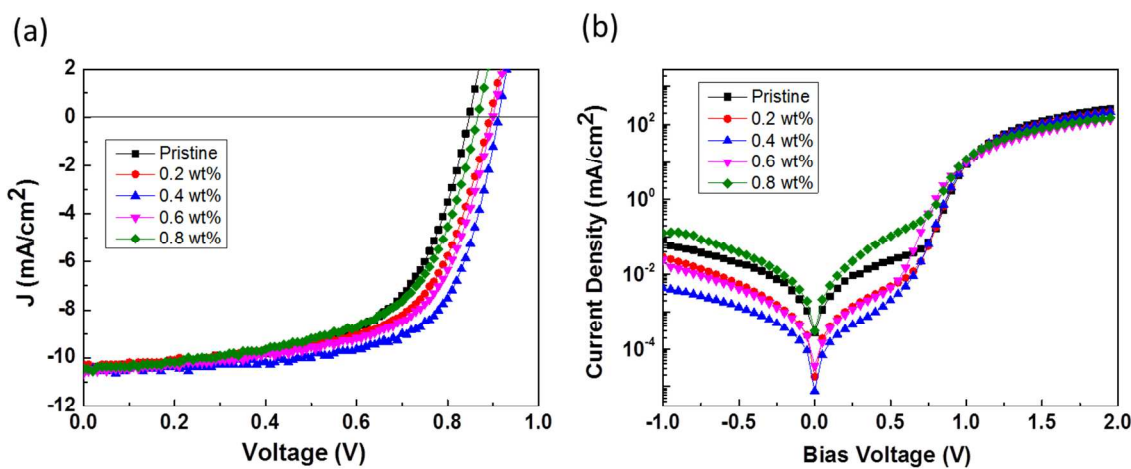


Figure 3. (a) Current density versus voltage characteristics of PCDTBT:PC<sub>71</sub>BM solar cells under 100 mW/cm<sup>2</sup> irradiation. (b) Dark current density versus voltage.

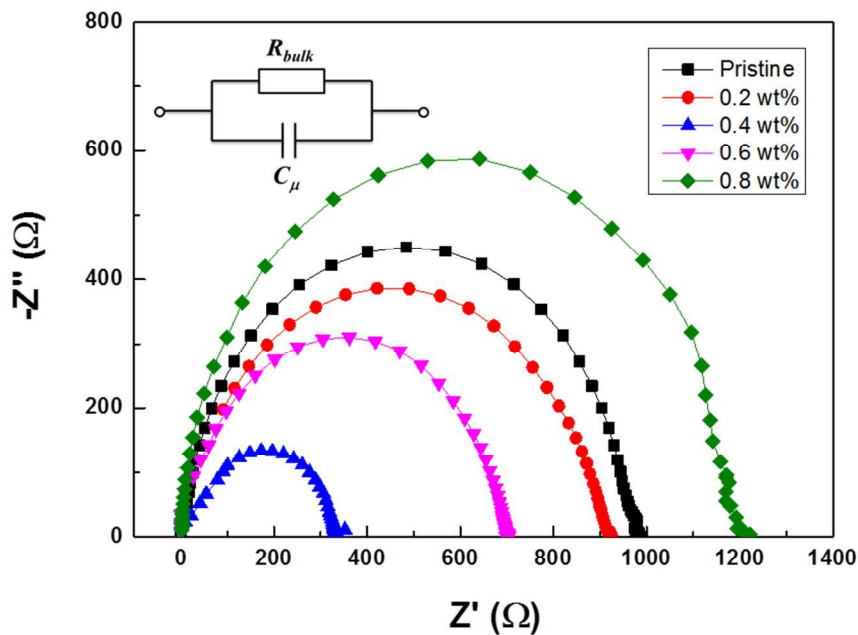


Figure 4. Nyquist plots of impedance spectra for PCDTBT:PC<sub>71</sub>BM solar cells without and with TFSA treatment at various concentrations and measured at the  $V_{oc}$  condition under dark. Inset shows the equivalent circuits of the devices, where  $R_{bulk}$  is the bulk resistance and  $C_\mu$  the chemical capacitance.

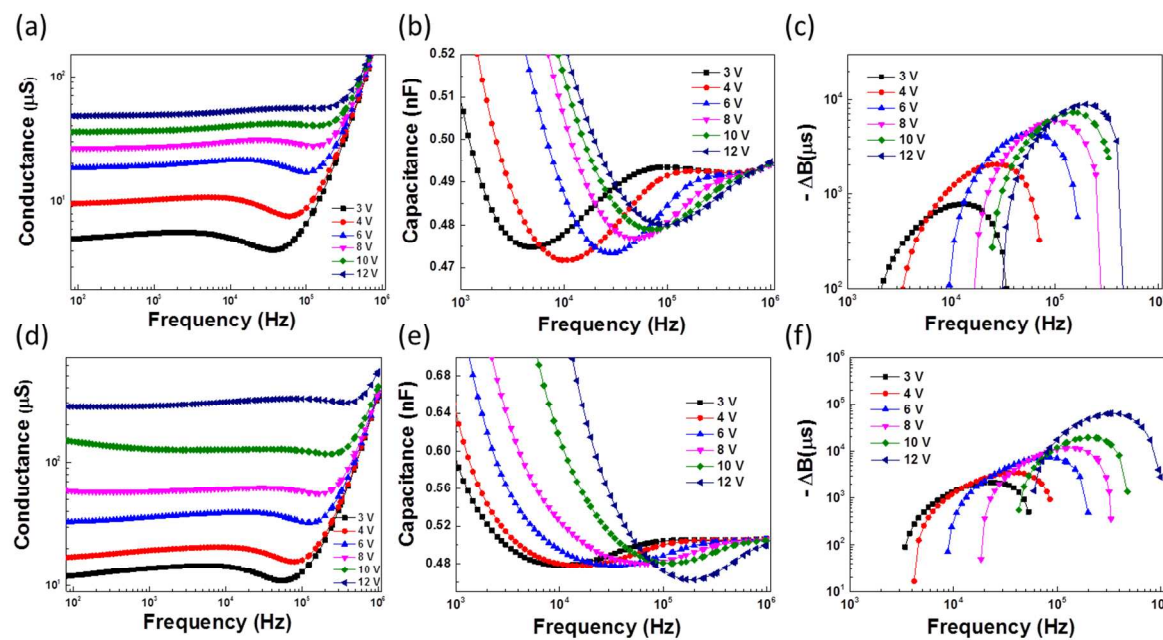


Figure 5. (a), (d) Conductance, (b), (e) capacitance and (c), (f) negative differential susceptances  $-\Delta B$  of pristine and 0.4% TFSA doped PCDTBT hole-only devices, respectively.  $-\Delta B$  is derived from capacitance data in (b), (d). by equation:  $-\Delta B = -\omega(C - C_{geo})$ , where  $f = \omega/2\pi$ ,  $C$  and  $C_{geo}$  are the frequency dependent and geometric capacitances of the organic film, respectively.

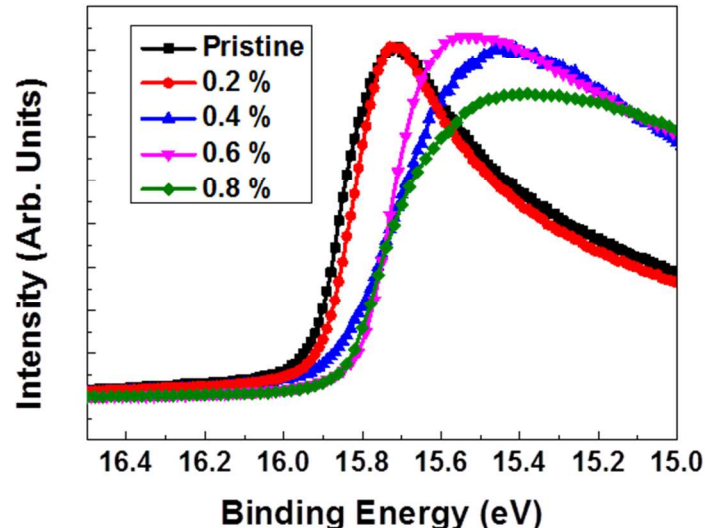


Figure 6. The UPS spectra of pristine and TFSA doped PCDTBT film at concentrations vary from 0.2 % to 0.8 %.

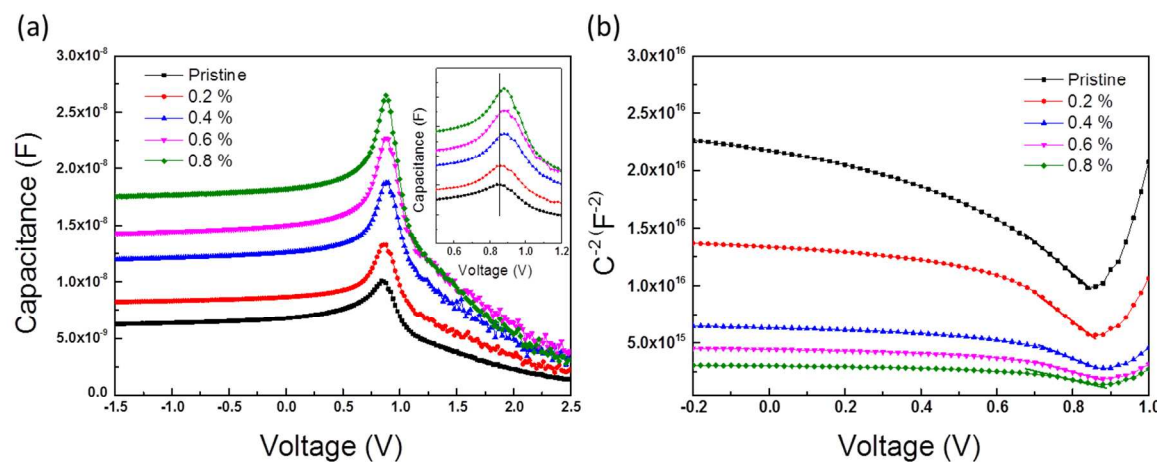


Figure 7 (a)  $C$ - $V$  characteristics and (b) Mott–Schottky curve of PCDTBT:PC<sub>71</sub>BM solar cells without and with TFSA treatment at various concentrations at frequency of 1k Hz. Inset in (a) displays the  $V_{bi}$  position at each conditions.

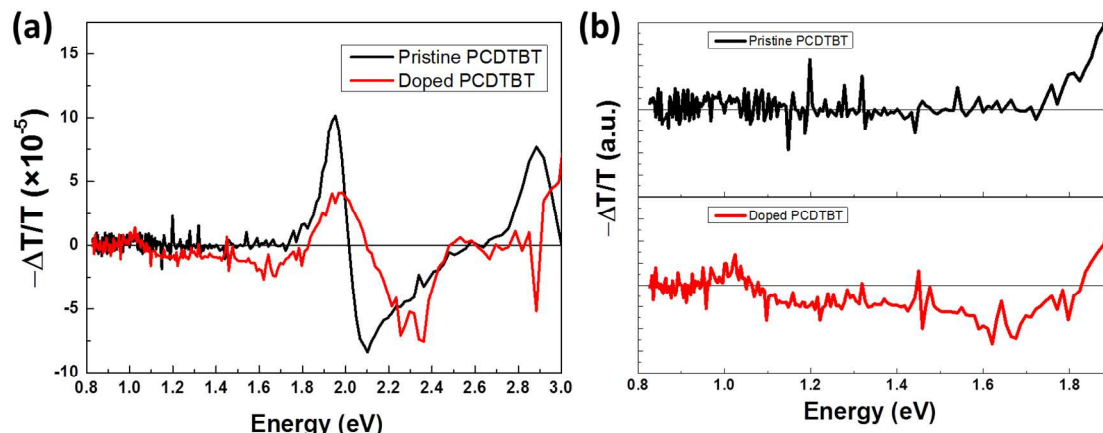


Figure 8 (a) The electroabsorption spectra of pristine and doped PCDTBT. (b) The sub-bandgap signal that zoomed from (a) at energy range from 0.8 to 1.9 eV.

Table 1. Photovoltaic parameters, hole concentration of PCDTBT:PC<sub>71</sub>BM solar cells and mobility of PCDTBT thin film with various TFSA dopant concentrations.

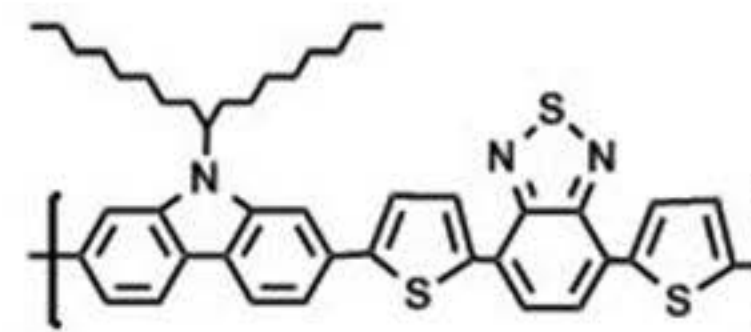
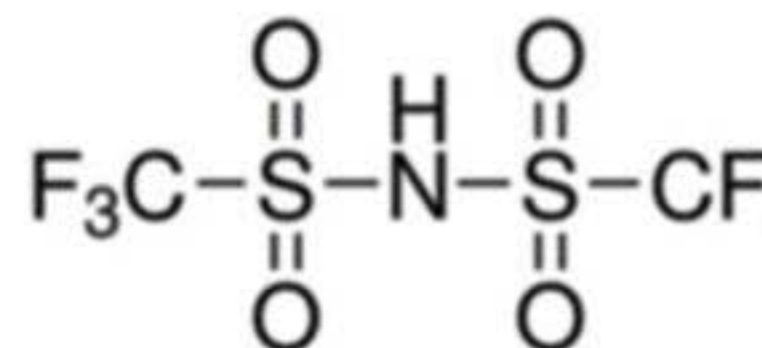
	$V_{oc}$ (V)	$J_{sc}$ (mA/cm <sup>2</sup> )	FF (%)	PCE. (%)	$N_A \times 10^{17}$ cm <sup>-3</sup>	Mobility $\times 10^{-4}$ (cm <sup>2</sup> /Vs)
Pristine	$0.85 \pm 0.02$	$10.5 \pm 0.1$	$60.7 \pm 0.1$	$5.39 \pm 0.01$	1.0	6.2
0.2 wt%	$0.89 \pm 0.02$	$10.3 \pm 0.2$	$63.0 \pm 0.4$	$5.76 \pm 0.01$	1.7	7.4
0.4 wt%	$0.91 \pm 0.01$	$10.5 \pm 0.1$	$67.3 \pm 0.2$	$6.46 \pm 0.03$	3.1	9.2
0.6 wt%	$0.90 \pm 0.02$	$10.6 \pm 0.1$	$62.2 \pm 0.3$	$5.96 \pm 0.02$	4.8	8.0
0.8 wt%	$0.87 \pm 0.03$	$10.5 \pm 0.2$	$59.2 \pm 0.5$	$5.37 \pm 0.04$	6.0	5.9

Average was obtained from over 20 devices tested.

Table 2. Carrier average mobility and average transit time from admittance spectroscopy analysis.

	Mobility $\times 10^{-4}$ (cm <sup>2</sup> /Vs)		Transit time (μs)	
	Pristine	0.4% Doped	Pristine	0.4% Doped
3 V	2.0	3.4	42.1	24.6
4 V	3.1	4.3	20.2	14.6
6 V	5.0	6.0	8.4	7.0
8 V	5.6	7.0	5.6	4.5
10 V	6.7	8.9	3.8	2.8
12 V	7.4	12.4	2.8	1.7

( a )



( b )

